Anal. Chem. **2008,** *80,* 4651–4658

Label-Free Detection of Single Protein Molecules and Protein−Protein Interactions Using Synthetic Nanopores

Anpan Han,[‡,†] Marc Creus,[§] Gregor Schürmann,[||,†] Vincent Linder,[⊥,†] Thomas R. Ward,[§] Nico F. de Rooij,[†] and Urs Staufer*[,†]

Institute of Microtechnology, University of Neuchâtel, Rue Jaquet-Droz 1, P.O. Box 526, CH-2002 Neuchâtel, Switzerland, and Department of Chemistry, University of Neuchâtel, Avenue de Bellevaux 51/C.P. 2, CH-2000 Neuchâtel, Switzerland

Nanofabricated pores in 20 nm-thick silicon nitride membranes were used to probe various protein analytes as well as to perform an antigen−antibody binding assay. A two-compartment electrochemical cell was separated by a single nanopore, 28 nm in diameter. Adding proteins to one compartment caused current perturbations in the ion current flowing through the pore. These perturbations correlated with both the charge and the size of the protein or of a protein−protein complex. The potential of this nanotechnology for studying protein−protein interactions is highlighted with the sensitive detection of β-human chorionic gonadotropin, a hormone and clinical biomarker of pregnancy, by monitoring in real time and at a molecular level the formation of a complex between hormones and antibodies in solution. In this form, the assay compared advantageously to immunoassays, with the important difference that labels, immobilization, or amplification steps were no longer needed. In conclusion, we present proof-of-principle that properties of proteins and their interactions can be investigated in solution using synthetic nanopores and that these interactions can be exploited to measure protein concentrations accurately.

The development of more sensitive assays for proteins is highly desirable as it will have a major impact in proteomics (i.e., for the understanding of the role of proteins in complex processes) and in clinical diagnostics (i.e., for alternative test formats). Classic immunoassays, which are routinely used for protein detection, have a sensitivity that is significantly lower than deoxyribonucleic acid (DNA) assays based on an amplification by means of polymerase chain reaction (PCR).[1] An elegant way to boost the sensitivity of protein assays is, hence, to use DNA as a label and employ DNA amplification, for example in immuno-PCR[2] or biobarcode assays,[3] which allow a significant decrease in the detection limits to a few tens of proteins.

In parallel to these developments, the detection of single biological molecules has become accessible using ultrasensitive fluorescence microscopy,[4–6] which, together with scanning probe microscopy (SPM),[7] is able to reveal inter- and intramolecular interactions and structural information.[8,9]

However, the above methods for protein analysis have inherent limitations, such as a requirement for labels, immobilization, or complicated instrumentation that may be overcome with nanopore-sensing.[10,11] Some unique advantages of using nanopores are (i) no labeling or immobilization of the analyte is necessary; (ii) the instrumental setup is simple and does not require any moving parts, and (iii) it allows real-time detection of the analyte. Nanopores are therefore well suited for studying proteins and interactions between proteins under native conditions and at the single molecule level.

Using the biological pore α-hemolysin, Meller et al. could distinguish DNA analytes which only differ in sequence.[11] However, biological pores have practical limitations due to operating pH, temperature, and fixed pore-diameter. Synthetic nanopores,[13–20] in contrast, are less affected by these parameters.

* Corresponding author. Current address: Dept. of Precision- and Microsystems Engineering, TU Delft, Mekel Weg 2, 2628 CD Delft, The Netherlands E-mail: u.staufer@tudelft.nl. Phone: 31 (0)15 278 6804.

† Institute of Microtechnology, University of Neuchâtel.

‡ Present address: Department of Micro and Nanotechnology, MIC, Technical University of Denmark, Copenhagen, Denmark.

§ Department of Chemistry, University of Neuchâtel.

|| Present address: Robert Bosch GmbH, Stuttgart, Germany.

⊥ Present address: Claros Diagnostics Inc, Woburn, Massachusetts U.S.A.

(1) Saiki, R. K.; Scharf, S.; Faloona, F.; Mullis, K. B.; Horn, G. T.; Erlich, H. A.; Arnheim, N. *Science* **1985**, *230*, 1350–1354.

(2) Sano, T.; Smith, C. L.; Cantor, C. R. *Science* **1992**, *258*, 120–122.

(3) Nam, J. M.; Thaxton, C. S.; Mirkin, C. A. *Science* **2003**, *301*, 1884–1886.

(4) Weiss, S. *Nat. Struct. Mol. Biol.* **2000**, *7*, 724–729.

(5) Mehta, A. D.; Rief, M.; Spudich, J. A.; Smith, D. A.; Simmons, R. M. *Science* **1999**, *283*, 1689–1695.

(6) Rigler, R.; Orrit, M.; Basche, T. *Single Molecule Spectroscopy, Nobel Conference Lectures*; Springer: Berlin, Germany, 2001.

(7) Bustamante, C.; Macosko, J. C.; Wuite, G. J. *Nat. Rev. Mol. Cell Biol.* **2000**, *1*, 130–136.

(8) Itoh, H.; Takahashi, A.; Adachi, K.; Noji, H.; Yasuda, R.; Yoshida, M.; Kinosita, K. *Nature* **2004**, *427*, 465–468.

(9) Noji, H.; Yasuda, R.; Yoshida, M.; Kinosita, K., Jr. *Nature* **1997**, *386*, 299–302.

(10) Kasianowicz, J. J.; Brandin, E.; Branton, D.; Deamer, D. W. *Proc. Natl. Acad. Sci. U.S.A.* **1996**, *93*, 13770–13773.

(11) Meller, A.; Nivon, L.; Brandin, E.; Golovchenko, J.; Branton, D. *Proc. Natl. Acad. Sci. U.S.A.* **2000**, *97*, 1079–1084.

(12) Dekker, C. *Nat. Nanotechnol.* **2007**, *2*, 209–215.

(13) Li, J.; Stein, D.; McMullan, C.; Branton, D.; Aziz, M. J.; Golovchenko, J. A. *Nature* **2001**, *412*, 166–169.

(14) Smeets, R. M.; Keyser, U. F.; Krapf, D.; Wu, M. Y.; Dekker, N. H.; Dekker, C. *Nano Lett.* **2006**, *6*, 89–95.

(15) Fologea, D.; Uplinger, J.; Thomas, B.; McNabb, D. S.; Li, J. *Nano Lett.* **2005**, *5*, 1734–1737.

10.1021/ac7025207 CCC: $40.75 © 2008 American Chemical Society
Published on Web 05/10/2008

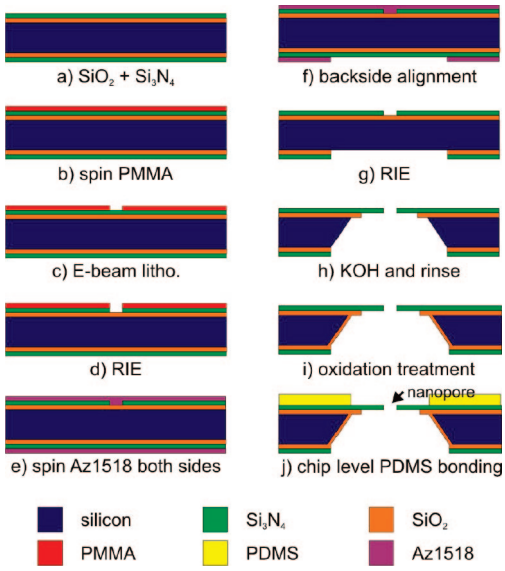

Figure 1. Nanopore fabrication flowchart, see text for details. Note that the dimensions of the chart are not drawn to scale.

For a recent review on solid state nanopores please refer to Dekker.[12] In spite of the apparent simplicity and elegance of the molecular Coulter counter, only DNA, nanoparticles,[21] and porphyrin[22] have been scrutinized with this methodology.

Stimulated by the potential applications of protein-translocation through nanopores, we recently reported for the first time on the detection of the protein bovine serum albumin (BSA) using nanopores fabricated by e-beam lithography.[23] Having established that single proteins could be detected by these means, we herein report the first demonstration, to our knowledge, that different proteins can be distinguished using nanopore-sensing, according to individual physicochemical properties, including size and pH-dependent migration. We also describe a proof-of-concept immunoassay that represents, to our knowledge, the first example of the detection of a specific protein−protein interaction with synthetic nanopores.

MATERIALS AND METHODS

Nanopore Fabrication Process. The nanopore fabrication is significantly improved compared to our previously reported work[23] in order to reduce the electrical capacitive load and, hence, increase the bandwidth. We started with dry thermal oxidation to form a 500 nm-thick silicon dioxide (SiO_2) layer on a 100 mm-diameter, ⟨100⟩ crystal orientation, 390 μm-thick, double sided polished silicon wafer. Then we coated the wafer on both sides with a layer of 20 nm-thick silicon nitride (Si_3N_4) (Figure 1a) by low pressure chemical vapor deposition (LPCVD). The wafer was treated in oxygen plasma (Tepla 132 from PVA Tepla, Feldkirchen, Germany. Parameters: rf power 1000 W, oxygen 400 mL/min, nitrogen 70 mL/min, pressure 0.73 mbar, 100 °C, 30 min) before spinning a polymethyl methacrylate (PMMA, 2% solid, MW 950 kDa, from MicroChem, MA) layer (1000 rpm, 60 s) onto the front side (Figure 1b). After spinning PMMA, the wafer was baked at 170 °C for 30 min. The e-beam lithography system, Raith 150, from Raith, Dortmund Germany, was used for PMMA exposure. To achieve the best wafer uniformity, the acceleration voltage was set to 20 kV, the aperture size was 7.5 μm, and the wafer was clamped onto an electrostatic wafer holder and leveled such that the electron beam was perpendicular to the wafer surface. The pores were patterned using the dot exposure mode (dose, 0.001 pAs) and other structures were written with the area exposure mode (dose: 150 μA/cm^2). After the exposure, the resist pattern was developed in a 1:3 methylisobutylketone (MIBK) to isopropanol mixture for 30 s and rinsed briefly in isopropanol and subsequently in deionized water (Figure 1c). The patterns in the PMMA were transferred into the Si_3N_4 by reactive ion etching (RIE), and the etching stopped on the SiO_2 by timing (Figure 1d). The RIE (Alcatel GIR 263, Annecy, France) used a SF_6/O_2 chemistry. Remaining PMMA was stripped in an oxygen plasma. A standard photolithography process was used to pattern the backside of the wafer: a 2.3 μm-thick AZ1518 photoresist (Shipley, Switzerland) was spun first onto the front side (to protect structures written by e-beam lithography) and then onto the backside of the wafer (Figure 1e). The photoresist on the backside served as a mask for the subsequent RIE (Figure 1f), which exposed the silicon on the backside of the wafer (Figure 1g). After the RIE, the photoresist was removed using oxygen plasma and subsequently the wafer was immersed into a 40% (m/v) KOH etch bath heated to 60 °C. The KOH created a free-standing membrane with the pore embedded (Figure 1h). After the KOH, 10 nm of SiO_2 was thermally grown at 950 °C before wafer dicing (Figure 1i). The membrane was situated in the middle of an 8 mm × 8 mm chip. To reduce the noise during current measurements, a 300 μm-thick polydimethylsiloxane (PDMS) sheet with a 200 μm diameter hole was prepared and sealed onto the silicon chip such that the membrane was under the hole (Figure 1j). Just before assay experiments, the chips were treated with a short (2 min) oxygen plasma to render the surface hydrophilic such that water was able to wet and fill the lumen of the nanopore. Immediately after the oxygen plasma, chips were immersed in water to avoid the PMDS losing its hydrophilic character upon exposure to air.

The fabrication results are shown in Figure 2. The pore diameter was measured to be between 20 and 30 nm using transmission electron microscopy (TEM).

Coulter Counter Model and Calculations. By combining Ohm's law and Maxwell's approximation for the conductivity of liquids with suspended insulating particles, Deblois and Bean[24]

(16) Heng, J. B.; Aksimentiev, A.; Ho, C.; Marks, P.; Grinkova, Y. V.; Sligar, S.; Schulten, K.; Timp, G. *Biophys. J.* **2006**, *90*, 1098–1106.
(17) Lanyon, Y. H.; De Marzi, G.; Watson, Y. E.; Quinn, A. J.; Gleeson, J. P.; Redmond, G.; Arrigan, D. W. M. *Anal. Chem.* **2007**, *79*, 3048–3055.
(18) Li, N. C.; Yu, S. F.; Harrell, C. C.; Martin, C. R. *Anal. Chem.* **2004**, *76*, 2025–2030.
(19) Harrell, C. C.; Lee, S. B.; Martin, C. R. *Anal. Chem.* **2003**, *75*, 6861–6867.
(20) Zhang, B.; Zhang, Y. H.; White, H. S. *Anal. Chem.* **2004**, *76*, 6229–6238.
(21) Lee, S.; Zhang, Y. H.; White, H. S.; Harrell, C. C.; Martin, C. R. *Anal. Chem.* **2004**, *76*, 6108–6115.
(22) Heins, E. A.; Siwy, Z. S.; Baker, L. A.; Martin, C. R. *Nano Lett.* **2005**, *5*, 1824–1829.
(23) Han, A.; Schürmann, G.; Mondin, G.; Bitterli, R. A.; Hegelbach, N. G.; de Rooij, N. F.; Staufer, U. *Appl. Phys. Lett.* **2006**, *88*, 093901.
(24) Deblois, R. W.; Bean, C. P *Rev. Sci. Instrum.* **1970**, *41*, 909.

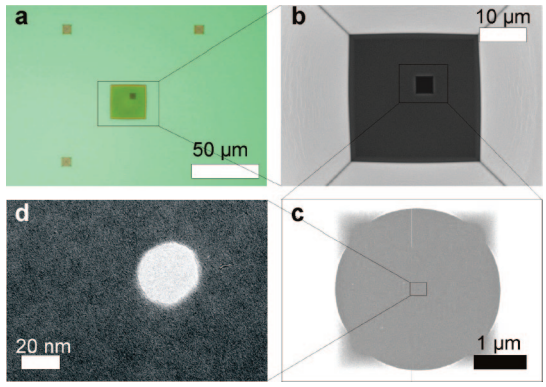

Figure 2. Fabrication results. (a) An optical microscope image of the SiO_2/Si_3N_4 membrane (front side of the wafer). A small dark square on the membrane equidistant from the three small squares is the membrane in Si_3N_4. (b) The SiO_2/Si_3N_4 membrane observed using SEM from the backside. (c) Zooming into the membrane in Si_3N_4 we observed a nanopore embedded in its center. (d) A high resolution TEM (200 keV) image of a characteristic pore.

and later Ito et. al[25] derived an expression for the current change (ΔI) caused by the translocation of a particle with the diameter, d_m, through a pore with diameter d_p and length l_p.

$$\Delta I = S(d_p, d_m)\frac{\kappa\pi U}{4(l_p + 0.8d_p)}d_m^{\,3} \qquad (1)$$

where U is the applied voltage, κ is the conductivity of the electrolyte solution, and $S(d_p, d_m)$ is a parameter depending on d_m and d_p. The current change is inverse proportional to the square of the dimensions of the pore. In our calculations we set the parameter $S(d_p, d_m)$ to unity.

Although the models for the ΔI are well established, we could not find models for the translocation time. This lack of published models probably reflects that the time resolution was never a problem, since l_p values were often above 10 μm.[24,25] However, in our case where l_p was about 20 nm, time resolution becomes a critical issue. Our experiments were carried out at very high ionic strength (1 M KCl) where the main transport mechanism of charged molecules subjected to an external electric field is electrophoresis.[26] Assuming a particle with the electrophoretic mobility μ_e passing through the pore at a velocity of $v = \mu_e U/l$,[26] the time, t, needed for translocation is

$$t = \frac{l}{v} = \frac{l^2}{\mu_e U} \qquad (2)$$

For 5 nm-large proteins dissolved in 1 M KCl, where the size of the particle is larger than the Debye length (L_D), μ_e is given by the Smoluchowski equation[26]

$$\mu_e = \frac{\varepsilon\zeta}{\eta} \approx \frac{\sigma L_D}{\eta} \qquad (3)$$

where ζ is the zeta potential, ϵ is the dielectric permittivity, σ is the surface charge density, and η is the viscosity. Menon et al. measured μ_e values for BSA at 10 mM NaCl, pH 8, to be 22×10^{-5}cm^2/V s. L_D at 1 M KCl is 0.3 nm which is 10 times smaller than at 10 mM.[26] Hence, according to 3, the mobility is reduced by a factor of 10. Inserting 20 nm for l, 0.1 V for U, and 2×10^{-5}cm^2/V s for μ_e, a BSA molecule will pass through the pore in 2 μs.

Apart from reducing the mobility of biomolecules, another advantage of working at very high ion concentrations is that the ζ potential of the walls of the nanopore itself is comparably small. The corresponding Debye length of the nanopore will also be in the range of 0.3 nm. Since the diameter of the nanopore is several nanometers larger than the diameter of the proteins being investigated, we could to a first approximation neglect pore−protein interactions.

Protein Samples and Their Preparation. Ovalbumin (OA) from chicken egg-white (pn, A7641), bovine serum albumin (BSA) (pn, A0281), and all chemicals were from Sigma unless specified. Avidin (AV) was from Belovo SA, Belgium,[27] and the preparation of recombinant streptavidin from *Escherichia coli* (SAV) is described by Humbert et al.[28] The antigen human chorionic gonadotropin β (β-HCG) from human pregnancy urine and the monoclonal anti-β-HCG antibody (pI 6.4) were from Fitzgerald, MA. Proteins were dissolved in 1 M KCl to 0.1 mg/mL and kept at 4 °C. KCl buffers (1 M) with different pH were adjusted to the same resistivity (9.09 Ω cm) using a conductivity meter (Orion 150, conductivity cell 012210, Boston, MA). We used 100 mM citrate buffer for pHs 2−6 and 100 mM bis-tris propane for pHs 7 and 8. The buffer pH was fine-adjusted using a sensitive pH meter (Orion 610, Boston, MA).

We investigated the solubility of SAV, AV, OA, and BSA at different pH. This was carried out by preparing 0.1 mg/mL protein solutions in buffers with different pH. If the proteins were not soluble at all, visible aggregates formed within an hour. Such pH conditions were unsuitable for nanopore experiments, since the risk of clogging the pores was very large.

Experimental Setup. A nanopore chip was mounted into an in-house designed cell made of Plexy glass, and both chambers were filled with buffer solution. The immersed Ag/AgCl electrodes were connected to a patch clamp amplifier (Axopatch 200B, Axon Instruments). Control experiments were performed such that we were certain that the current that we measured was conducted through the nanopore.[23] By measuring the current, we could calculate the diameter of the pore.[23] The average diameter calculated for wafer A was 24.4 ± 2.8 nm (14 chips), and 27.9 ± 1.4 nm (12 chips) for wafer B, which was in agreement with transmission electron microscope (TEM) measurements. For OA experiments, pores from wafer A were used, and wafer B was used for all other experiments.

Only one protein was analyzed per chip to avoid cross-contamination. Each nanopore experiment started with a clean chip. With the trans electrode biased at 50 mV, if the current for a clean chip was stable and the noise was below 20 pA (root-mean-square, 10 ms window, 100 kHz low-pass filter) the chip could be used. More than 50% of the chips were suitable for experiments; a yield of more than 50% on a wafer level is generally considered as excellent for a prototype.

(25) Ito, T.; Sun, L.; Crooks, R. M. *Anal. Chem.* **2003**, *75*, 2399–2406.
(26) Shaw, D. J. *Introduction to Colloid and Surface Chemistry*, 4th ed.; Butterworth-Heinemann: Oxford, U.K., 1989.
(27) Hiller, Y.; Gershoni, J. M.; Bayer, E. A.; Wilchek, M. *Biochem. J.* **1987**, *248*, 167–171.
(28) Humbert, N.; Zocchi, A.; Ward, T. R. *Electrophoresis* **2005**, *26*, 47–52.

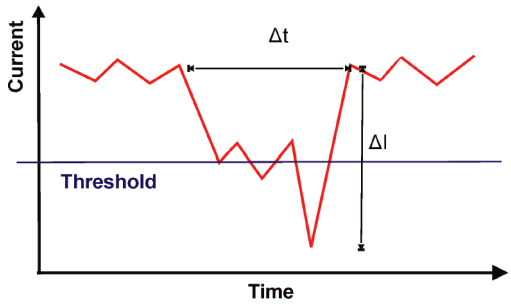

Figure 3. Data analysis, schematically indicating how the spike-duration time Δt and the current drop ΔI were defined. See text for details.

Current recordings were made with several voltage biases. Before changing the pH, we rinsed the chambers with water and made current recordings to ensure that the protein was indeed removed by washing. The number of spikes decreases by more than 90% after washing. For the pH sweeps, we started from pH 6 and stepped down to pH 2. To get a reasonable number of spikes, higher protein concentrations (up to 10 μg/mL) were needed at lower pH. By starting at low concentrations, carry-over of proteins between experiments was less problematic. We then carried out experiments at pHs 7 and 8. The number of spikes detected was proportional with the protein concentration (results not shown), which justified the use of normalization. We did not use concentrations higher than 10 μg/mL, since the carry-over between experiments could be very large.

Data Handling and Treatment. The analog signal from the patch clamp amplifier was digitized using a data acquisition card from National Instruments (PCI 6052E), and Labview software (LV) was used to control the data acquisition card and later on to perform signal processing. The acquisition rate was set to 300 kHz, and the data were directly saved to the hard drive. During data processing, the following routine was used. The data from the hard-drive were read, and the data were globally leveled such that minor drifts of the experiment were eliminated. Spikes were extracted from the leveled data. The duration, Δt, and maximal current drop, ΔI, were obtained (Figure 3). The use of maximal current drop was preferred for data processing because, although background noise is directly added, it is a very simple method to implement. The less noisy, alternative method would have been to average data points at the bottom of a valley, which, however, would have been more evolved due to the many different shapes of the spikes.

RESULTS AND DISCUSSION

Homogenous Protein Translocation. According to our estimate, at pH 8 a BSA molecule should transit through a 20 nm long nanopore in 2 μs (See Materials and Methods). To measure 2 μs current perturbations, the measurement bandwidth should be at least 1 MHz. To increase the time resolution, we improved our previously reported nanopore design[23] such that the measurement bandwidth increased from 5 to 100 kHz, which is the maximum bandwidth of our state-of-the-art patch clamp amplifier from Axon Instruments. Our time resolution is 10 times better compared to previous reports.[15,29,30] Still, this improvement only

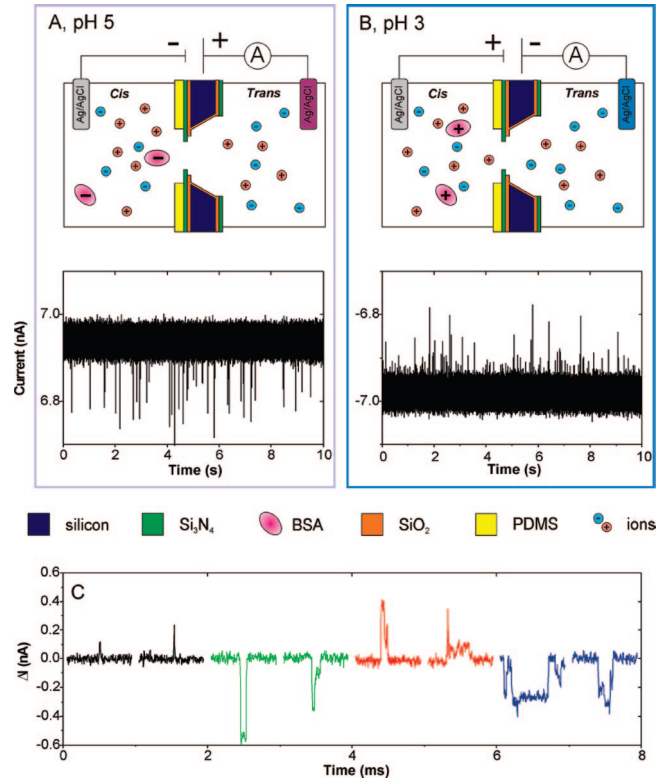

Figure 4. Protein translocation experiment: After insertion of a chip containing the nanopore, buffer was added into both chambers and the ion current was measured using a low-noise current amplifier. Measurement bandwidth was 100 kHz; at 10 kHz most current perturbations were not resolved. (A) At pH 5, BSA was added to the cis chamber; valleys were observed in the current transient when the trans electrode voltage was set to 50 mV. Very few peaks were observed at −50 mV. (B) At pH 3, the opposite was observed for BSA: peaks dominated at −50 mV compared to valleys at 50 mV. (C) Trace of high time-resolved current change of selected perturbations, BSA at pH 3 with −50 mV bias (black line), BSA at pH 6 with 50 mV bias (green line), AV at pH 6 with −50 mV bias (red line), and SAV at pH 5 with 50 mV bias (blue line).

provided a practical time resolution of 40 μs. To further increase the resolution of translocation events, the electrophoretic mobility (μ_e) of the protein analyte was decreased by operating at a pH closer to its isoelectric point (pI), where the protein has zero net-charge. We carried out measurements at various pH for four different proteins: ovalbumin (OA), avidin (AV) from egg white, BSA, and recombinant streptavidin (SAV) expressed in *Escherichia coli*.[28] After adding a protein sample to the cis side of the pore, the current was recorded when the trans electrode was biased at +50 mV and then at −50 mV (an example of BSA is in Figure 4A,B). To describe the polarity of the perturbations clearly and for the avoidance of doubt we define current perturbations that increased the current as peaks, and perturbations that decreased the current as valleys. We observed that the fine-detail of current perturbations (zooming in) had different shapes (Figure 4C). For BSA, at pH far away from pI, most perturbations were very sharp and the duration of such events was often less than 40 μs. Hence, the fine-detail of current perturbations could not be resolved at pH values far from the pI, due to our electronics' inability to detect

(29) Storm, A. J.; Storm, C.; Chen, J.; Zandbergen, H.; Joanny, J.-F.; Dekker, C. *Nano Lett.* **2005**, *5*, 1193–1197.

(30) Li, J. L.; Gershow, M.; Stein, D.; Brandin, E.; Golovchenko, J. A. *Nat. Mater.* **2003**, *2*, 611–615.

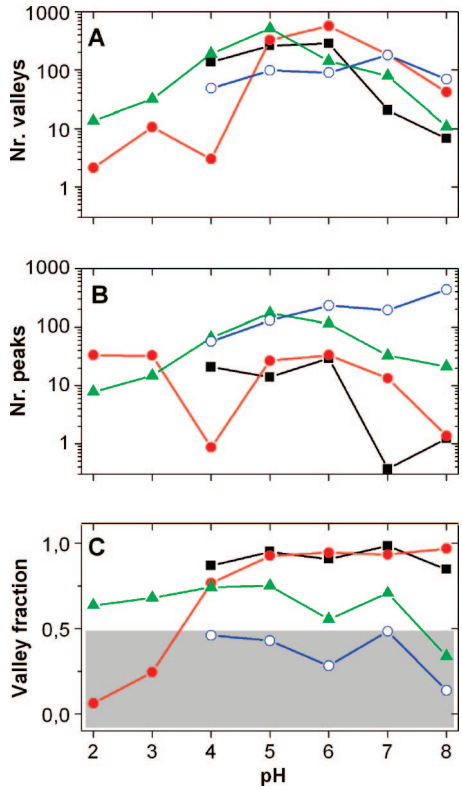

Figure 5. Number of (A) valleys and (B) peaks counted during 1 min for OA (■), BSA (red ●), SAV (green ▲), and AV (blue ○) at different pH. Valley fraction, f_v, is given in part C (see Supporting Information for data used to generate Figure 5). Note that the error for the calculated f_v for BSA at pH 4 is very high, since we only had less than 10 data points.

fast translocations. In contrast, at pH closer to the p*I*, perturbations had rough shapes and more complex structures. These observations agreed well with our model.

The number of detected valleys and peaks was plotted against the pH (Figure 5A,B). Each data point was based on the average value of three experiments performed in three different pores. In total, 12 different pores were used for the experiments reported in Figure 5. We have not been able to obtain any data for OA and AV at pHs 2 and 3 due to protein aggregation (see Materials and Methods for details). The number of perturbations counted during 1 min was normalized with the protein concentration in the cis chamber (μg/mL). The unit in full is (number of perturbations)/minutes/(μg protein/mL). To compare the number of peaks and valleys detected at a given pH, we plotted the fraction of current perturbations identified as valleys, $f_v = n_v/(n_p + n_v)$, where n_v is the number of valleys and n_p is the number of peaks (Figure 5C).

The average time duration of respectively valleys (Δt_{valley}) and peaks (Δt_{peak}) is reported in Figure 6.

We postulate that the current perturbations shown in Figure 4 are caused by single protein molecules translocating through the pore. As the protein passes through the pore, some ions are prevented from translocating across the pore, decreasing the absolute current and causing current perturbations in the current trace. Protein molecules with a negative net-charge are driven to the positively biased trans electrode, causing a current drop (a valley); conversely, positively charged proteins are driven toward the negatively biased electrode. According to our postulate, if $f_v = 1$, all proteins in a sample are negatively charged, if $f_v = 0$,

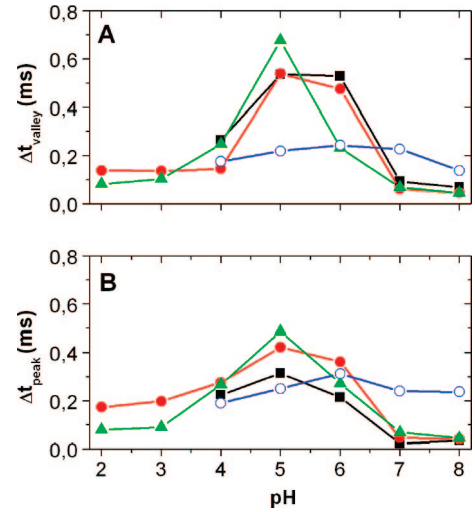

Figure 6. The time duration of each current perturbation (■ OA; (red ●) BSA, (green ▲) SAV, and (blue ○) AV) was extracted and the averaged duration of valleys and peaks was obtained for different pH.

all proteins are positively charged, and if $f_v = 0.5$, half of the proteins are positively charged and the other half is negative.

Experiments performed with BSA support our interpretation that current perturbations are caused by translocating proteins and justify our initial concern that they must be slowed down to allow their detection: (i) The longest average current perturbation durations for BSA were observed around its p*I*, where the analyte has lowest mobility (Figure 6). (ii) At low μ_e, our electronics were sufficiently fast to detect protein translocation; more current perturbations were detected when experiments are performed at a pH close to the p*I* (Figures 5 and 6). Only a fraction of the protein translocations were detected at other pH values. For BSA, most current perturbations were detected at pH 6, while for high or low pHs, fewer current perturbations are apparent (Figure 5A,B). In addition, the average current perturbation duration was largest for pHs 5 and 6 (Figure 6). This observation was also confirmed with OA. At high pH, over 90% of the current perturbations were valleys, whereas mostly peaks were observed at pHs 2 and 3 (Figure 5C). At pH 4, close to BSA's isoelectric point, very few current perturbations (<10) are detected. Our results and interpretations for BSA agreed with previous reports using different techniques which suggest that BSA is negatively charged at pH > 4.25, while positively charged below this pH.[31–33] The fact that the switch of polarity did not take place at pH 5.3, the p*I* measured by isoelectric focusing, may be explained by BSA having a pronounced affinity for anions.[31–33] According to Scatchard et al. and Menon and Zydney,[32,33] at pH 5 while being slightly positively charged at 1 mM Cl^-, BSA binds up to 8 Cl^- ions at 50 mM Cl^- resulting in a negative net-charge. Consequently, we interpret that at pH 4, BSA carries almost zero net-charge and is therefore only marginally affected by the applied electric field, which agrees well with our observation that at pH 4 only few current perturbations are detected.

We expected AV, generally believed to exhibit a p*I* of 10.5, to be positively charged across the whole pH range. However,

(31) Norde, W.; Lyklema, J. J. *Colloid Interface Sci.* **1978**, *66*, 277–284.
(32) Menon, M. K.; Zydney, A. L. *Anal. Chem.* **1998**, *70*, 1581–1584.
(33) Scatchard, G.; Coleman, J. S.; Shen, A. L. *J. Am. Chem. Soc.* **1957**, *79*, 12–20.

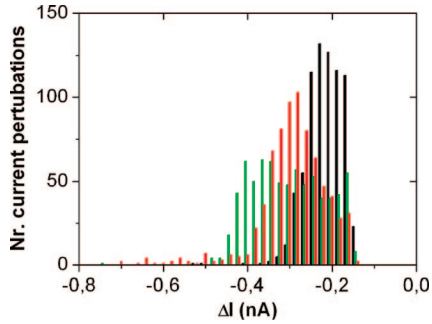

Figure 7. Statistical analysis of the distribution of current drop for OA (black), BSA (red), and SAV (green) at pH 6. Driving voltage 100 mV; 750 events for each protein.

according to our results, AV only clearly showed a positive charge at pH 8, and the ratio f_v was about 0.5 for pH between 4 and 7 (Figure 5C). This finding is explained by the fact that the egg-white avidin is highly heterogeneous both in terms of molecular weight and glycosylation,[27] leading to a protein population with both positive and negative charge at the same pH. Homogeneous, nonglycosylated recombinant SAV[28] would be expected to switch polarity at pH 6 or 7 (calculated p*I*), but puzzlingly, most SAV molecules appeared to maintain an overall negative charge across the whole pH scale. Although the recombinant SAV was initially judged pure by sodium dodecyl sulfate-polyacrylamide gel electrophoresis (SDS-PAGE) and electrospray ionization time-of-flight (ESI-TOF) mass spectrometric analysis,[28] isoelectric focusing experiments reveal that both AV and SAV contained several species with varying p*I* (results not shown). These results suggest that analysis based on the Coulter principle in nanopores is exquisitely sensitive to protein microheterogeneity, as it is performed at the molecular level, in solution, under nondenaturing conditions.

Statistical analysis of the current change ΔI of the valleys, i.e., depth of the valleys at pH 6 (Figure 7) showed one clear maximum for OA and BSA, while the distribution for SAV was broader. On average, BSA (67 kDa) caused a larger current drop than OA (43 kDa). This observation also supports the interpretation that each current perturbation corresponded to a single protein translocation since, according to the Coulter principle, larger molecules yield a larger current drop.

We performed statistical analyses for each pore and protein from which the most frequent current drop ΔI_{mf} was obtained. The current drop is proportional to the third power of the particle diameter (d_m) (eq 1), which allowed estimating an upper value for d_m of BSA and OA (see Table 1). As expected, the BSA has a larger diameter than OA. Excellent reproducibility was observed between experiments performed using different pores at different times. The variation of ΔI_{mf} is equivalent to the upper limit of the variation of d_m^3. The 10% ΔI_{mf} variation for proteins 5 nm in diameter (OA) corresponds to just 2 Å variation in diameter. Hence, we could reproducibly determine the diameter of BSA and OA with a variation less than 2 Å, which is equivalent to 2 hydrogen atoms side by side. We calculated an upper value for the protein diameter because our analysis is based on the largest magnitude of each peak (see Materials and Methods). This may explain the difference between the protein diameter measured by our experiments (7.3 and 8.6 nm) and those obtained from sedimentation equilibrium studies (5.4 and 7.1 nm).[34]

Table 1. Baseline Current, I_b, ΔI_{mf}, and Calculated Values for Pore, d_p, and Protein Diameter, d_m

pore	protein	I_b (nA)	d_p (nm)[a]	ΔI_{mf} (nA)	d_m (nm)
A	OA	10.7	21.9	0.21	7.1
B	OA	10.8	22.0	0.25	7.5
C	OA	14.0	26.3	0.23	7.3
D	BSA	14.0	26.4	0.31	8.6
E	BSA	14.5	26.5	0.27	8.7
F	BSA	15.9	28.9	0.31	8.8

[a] Calculated values of pore diameter.[23] From sedimentation equilibrium studies the diameters of OA and BSA are, respectively, 5.4 and 7.1 nm.[34]

Protein−Protein Interactions. Having established that proteins could be detected using synthetic nanopore and having investigated the detection characteristics according to protein size and pH, we wondered what would happen if two proteins with mutual specific affinity were probed with the nanopore. We set out to detect a specific protein−protein interaction: antigen−antibody binding.

Abundance of the antigen β-human chorionic gonadotropin (β-hCG) in women's urine is diagnostic of pregnancy. In the first experiments, we added monoclonal anti-β-hCG antibody from mouse (IgG) to the cis chamber to a final concentration of 4 μg/mL at pH 6, whereupon translocation experiments we observed large valleys. Then we washed the cis chamber and added a solution containing both β-hCG and the antibody, which was incubated for 1 h at room temperature. Only very few current perturbations were detected for this sample. To further investigate the specificity of this phenomenon, the experiment was repeated by adding first the antibodies (Figure 8A) and then another, noninteracting protein (OA) (Figure 8B). We observed large valleys caused by the antibody and smaller valleys caused by OA. Then, β-hCG was added to a final concentration of 1 μg/mL, at which point the large valleys could not be detected, whereas the small current perturbation associated with OA remained (Figure 8C). Finally, a dose−response curve was obtained by adding aliquots of the antigen to the antibody in the cis chamber. The number of valleys with current drop above 0.4 nA was counted during 1 min and is plotted in Figure 8D. We observed that the number of valleys decreased with increasing concentrations of β-hCG; furthermore, above 1 μg/mL of β-hCG, the change approached saturation.

From the above experiments, one would anticipate an increase in the current perturbation magnitude when probing the sample containing antibody to which antigens have been added, since the formed protein complex is larger than the antibody. Strikingly, we observed a reduction in the number of current perturbations, which must be due either to the inhibition of protein translocation or, if proteins could translocate, to the inability of our system to detect their translocation under these conditions. From the experiments where OA was added to the sample, we conclude that (i) the pore remained functional after antigen addition. Indeed, since OA translocations were still detected, no clogging of the pore occurred. (ii) While the addition of OA did not affect IgG

(34) Cabre, F.; Canela, E. I.; Canela, M. A. *J. Chromatogr.* **1989**, *472*, 347–356.

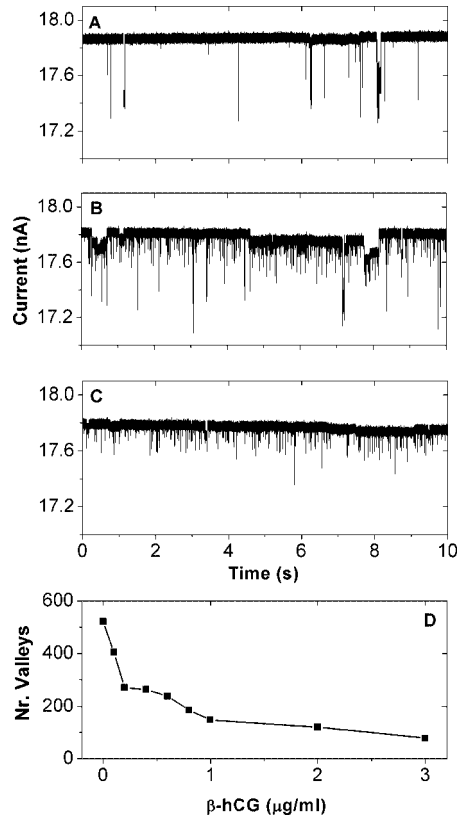

Figure 8. Antibody−antigen binding-experiment. (A) Monoclonal anti-β-hCG antibody was added to the cis chamber. (B) Then OA was also added to the cis chamber. (C) Finally, β-hCG was added. (D) Dose−response curve. The line is added to guide the eye.

translocation, the antigen strongly decreased the number of large valleys. Hence, the absence of valleys upon antigen addition to the chamber already containing antibody was caused by a specific interaction between antibody and antigen. As the size of the antigen−antibody complex is expected to remain smaller than the nanopore's diameter, we speculate that the absence of antibody-associated valleys upon addition of antigen was due to a change of the electrophoretic mobility μ_e of the antibody when bound to β-hCG. While, IgG has a p*I* around 6 and the p*I* for β-hCG is about 3,[35] it is likely that upon IgG binding to two β-hCG the μ_e is strongly increased such that the electronics were not able to detect the fast translocation events. For experiments of IgG carried out at pH 7, only 45 valleys were detected per minute, compared to the 500 valleys at pH 6. This supports the assumption that the antigen−antibody complex has an increased mobility compared to free antibody at the pH tested. On the basis of our experiments for four different proteins at different pH, an obvious experiment to verify, that indeed the antigen−antibody complex has higher mobility, is to carry out an assay at low pH, where our electronics will have sufficient bandwidth to detect the translocating complex. However, in the case of antibody−antigen interaction, low pH is known to disrupt the complex, making such verification studies impossible. Furthermore, since β-hCG has a molecular weight of about 20 kDa and IgG about 150 kDa and there are two binding sites per monoclonal IgG, then we would expect full saturation of the antibody (4 μg/mL) at around 1 μg/mL of antigen. Accordingly, we observed in the dose response plot (Figure 8D) a plateau of saturation at 1 μg/mL of antigen. This dose response, consistent with the known specificity of antibody−antigen interactions, supports the notion that synthetic nanopores can be used for immunoassays or protein complex assays.

Since binding to another protein with more mobility appears to increase the mobility of the protein, our assay can be compared to mobility shift assays, which is a frequently used gel-based assay, e.g., to investigate the binding of gene regulating proteins to DNA.[36] Similar assays to determine molecular interactions are also found in capillary electrophoresis.[37]

CONCLUSION

An unmatched and unique advantage of this nanopore-based protein assay is that no label or sample immobilization is required. In most protein−protein binding assays, either labeling and/or sample immobilization or a subsequent signal generation/amplification step is needed.[38] Directly labeling the protein may lead to loss of binding-affinity and sensitivity, and moreover, labeling and signal amplification processes can be costly and time-consuming.[38] Label-less technologies such as surface plasmon resonance[39] and mass sensitive piezoelectric biosensors[40] do not require direct labeling of proteins; however, ligands or binding partners require covalent immobilization or physical adsorption to the sensor surface, which could ultimately modify the binding kinetics and in the worst case lead to a short fall of specific molecular interactions. In contrast and complementary to the above techniques, nanopore sensing allows sensitive and direct detection of single molecules in solution.

The number of molecules needed for analysis is equivalent to the statistical reliable count of molecules, i.e., less than 1000 molecules. The relationship between detection events and the concentration of analyte in the cis chamber is crucial for understanding the sensitivity of a nanopore-based assay: the count-rate reflects the probability that an individual molecule reaches the nanopore. At low concentrations, translocation to the vicinity of the pore takes a long time and, consequently, the nanopore shares the fate of other exquisitely sensitive detectors like single fluorescent photon detection, where a molecule is only detected if it reaches the focal area. Ultimately, only diffusion and the time of measurement limit the sensitivity of the assay. Assuming the sensitivity is diffusion limited, we could estimate the practical detection limit of a nanopore assay. With application of Poisson and Gaussian statistics, the standard deviation of 1000 counts is the square root of 1000 which is 32 counts, corresponding to a coefficient of variation (CV) of 3.2%. Therefore, to determine a concentration with a CV of less than 3.2% it is required to count at least 1000 molecules. On the basis of our current count rate, which is about 500 counts/min for an antibody concentration of 25 nM, and limiting the counting time to 10 min, we could measure

(35) Sigma-Aldrich, Product Number C 0434.

(36) Fried, M. G. *Electrophoresis* **1989**, *10*, 366–376.
(37) Heegaard, N. H. H. *Electrophoresis* **2003**, *24*, 3879–3891.
(38) Kricka, L. J.; Wild, D. In *The Immunoassay Handbook*, 3rd ed.; Wild, D., Ed.; Elsevier: Amsterdam, The Netherlands, 2005, pp 192−230.
(39) Jonsson, U.; Fagerstam, L.; Ivarsson, B.; Johnsson, B.; Karlsson, R.; Lundh, K.; Lofas, S.; Persson, B.; Roos, H.; Ronnberg, I.; Sjolander, S.; Stenberg, E.; Stahlberg, R.; Urbaniczky, C.; Ostlin, H.; Malmqvist, M. *Biotechniques* **1991**, *11*, 620.
(40) Janshoff, A.; Galla, H. J.; Steinem, C. *Angew. Chem., Int. Ed.* **2000**, *39*, 4004–4032.

a 5 nM antibody solution with 3.2% CV. In certain applications, when a CV of 10% is sufficient, then 100 counts are required. This accuracy allows the measure of down to 0.5 nM in 10 min. However, in the case of detection of complexes, affinities will also determine the sensitivity of the assay.

We show that synthetic nanopores can be used for detecting proteins and complexes and to measure protein characteristics, such as size and p*I*, which can be exploited for accurate and sensitive protein−protein bioassays. We believe that it would be feasible to determine the absolute size of protein molecules with high reproducibility by correlating more detailed nanopore protein interaction models with translocation studies using carefully prepared protein samples with different molecular weight. Together, these findings open new paths for novel applications in biotechnology.

Finally, we were intrigued to observe reproducible structures in the fine detail of current perturbations at pH close to the p*I* of proteins, at conditions where the migration of proteins is postulated to be slower. We speculate that such complex shapes may provide valuable structural information of macromolecules in solution, further expanding the usefulness of synthetic nanopores. Such experiments, to explore the fine structure of the signals observed, form the basis of our future investigations.

ACKNOWLEDGMENT

The authors would like to thank the technical staff of ComLab, the joint IMT-CSEM clean room facility, and Massoud Dadras and Peter Van der Wal for helpful discussions. Anpan Han also acknowledges the Danish Research Agency for the financial support (Grant Internationaliseringsstipendium). This project was financially supported by the République and Canton de Neuchâtel. The authors declare that they have no competing financial interests.

SUPPORTING INFORMATION AVAILABLE

Data for Figure 5. This material is available free of charge via the Internet at http://pubs.acs.org.

Received for review December 12, 2007. Accepted March 17, 2008.

AC7025207